Toward Understanding the Simulated Phase Partitioning of Arctic Single-Layer Mixed-Phase Clouds in E3SM

Meng Zhang[1], Shaocheng Xie[2], Xiaohong Liu[1*], Wuyin Lin[3], Kai Zhang[4], Hsi-Yen Ma[2], Xue Zheng[2], Yuying Zhang[2]

[1] Department of Atmospheric Sciences, Texas A&M University, College Station, Texas, USA

[2] Lawrence Livermore National Laboratory, Livermore, CA, USA,

[3] Brookhaven National Laboratory, Upton, NY, USA,

[4] Pacific Northwest National Laboratory, Richland, WA, USA

* Correspondence to X. Liu, xiaohong.liu@tamu.edu

Key Points:

- EAMv1 simulated Arctic single-layer mixed-phase clouds are overly dominated by supercooled liquid with little ice produced;
- Reduced heterogeneous ice nucleation by CNT from Meyers scheme at warm temperatures is responsible for the underestimate of ice formation;
- Lacking the ice phase processes in CLUBB and its interaction with stratiform cloud microphysics limits the growth of cloud ice.

Abstract

Arctic mixed-phase clouds simulated by the U.S. Department of Energy (DOE) Energy Exascale Earth System Model (E3SM) Atmosphere Model version 1 (EAMv1) are found to be overly dominated by supercooled liquid with little ice production. Sensitivity experiments using the short-term hindcast approach are performed to isolate the impact of several new parameterizations on the simulated mixed-phase clouds in EAMv1. These include the Classical Nucleation Theory (CNT) ice nucleation scheme, the Cloud Layer Unified By Binormals (CLUBB) parameterization, and the updated Morrison and Gettelman microphysical scheme (MG2). Results are compared to the DOE's Atmospheric Radiation Measurement (ARM) Mixed-Phase Arctic Cloud Experiment (M-PACE) observations. It is found that all of these new parameterizations are responsible for the decrease of cloud ice water content in EAMv1 simulated single-layer mixed-phase clouds. A budget analysis of detailed cloud microphysical processes suggests that a lack of initial ice particles from ice nucleation or convective detrainment strongly diminishes the cloud ice water content through the subsequent ice mass growth processes. Reduced heterogeneous ice nucleation by CNT at temperatures warmer than -15℃ along with negligible ice processes in CLUBB are primarily responsible for the problem. Because the use of MG2 does not impact initial ice formation, the MG2 cloud microphysics is not the primary reason for the underestimate of cloud ice. However, using MG2 leads to a lower total ice mass due to a higher accretion rate of liquid droplets by rain drops and a lower ice mass growth rate.

1. Introduction

Mixed-phase clouds, which are composed of both ice crystals and supercooled liquid droplets, are one of the most frequently observed clouds during the spring and fall seasons in the Arctic (de Boer et al., 2009; Shupe et al., 2006, 2011; Zhang D. et al., 2019). They have large impacts on the sea ice and ice sheet melt (Bannartz et al., 2013; Hofer et al., 2019; Nicolas et al., 2017) along with regional and global climate changes (Lawson & Gettelman, 2014; Lohmann & Neubauer, 2018; Tan & Storelvmo, 2019). The phase partitioning between liquid and ice water in mixed-phase clouds can substantially impact the radiative fluxes at the surface and alter the surface energy budget due to the vastly different optical properties between liquid droplets and ice crystals (Bannartz et al., 2013; Hofer et al., 2019; Nicolas et al., 2017).

It is imperative for general circulation models (GCMs) to accurately capture the microphysical properties of mixed-phase clouds in order to achieve a reliable future climate prediction. However, large uncertainties remain in the modeling of mixed-phase clouds in current GCMs (Barrett et al., 2017; Klein et al., 2009; Komurcu et al., 2014; Morrison et al., 2009). For example, the temperature at which the amount of cloud liquid water and ice water is equally abundant in the simulated mixed-phase clouds over the Southern Ocean varies by 40℃ among 19 Coupled Model Intercomparison Project Phase 5 (CMIP5) models (McCoy et al., 2015, 2016). One challenge in modeling mixed-phase clouds lies in the representation of heterogeneous ice nucleation that occurs at temperatures warmer than -37℃ (Liu et al., 2011; Shi & Liu, 2019; Xie et al., 2008, 2013). The heterogeneous ice nucleation parameterizations commonly used in current GCMs are derived from laboratory measurements (DeMott et al., 2015; Niemand et al., 2012), field observations (DeMott et al., 2010), or are based on the

64 Classical Nucleation Theory (CNT) (Hoose et al., 2010; Wang et al., 2014). However,
65 considerable uncertainties in simulated ice particle number concentration of mixed-phase clouds
66 remain due to the poor representations of atmospheric processes of ice nucleating particles
67 (INPs) (Shi & Liu, 2019) and secondary ice production in mixed-phase clouds (Field et al.,
68 2017). Another challenge exists in the treatment of ice depositional growth through the Wegner-
69 Bergeron-Findeisen (WBF) process in mixed-phase clouds. In the WBF process, ice particles
70 grow at the expense of coexisting liquid droplets because of the lower equilibrium vapor pressure
71 with respect to ice than that with respect to liquid at temperatures colder than 0℃. It has been
72 found that the simulated phase partitioning in mixed-phase clouds is strongly sensitive to the
73 treatment of the WBF process in GCMs. The representation of the WBF process in current
74 GCMs often ignores subgrid cloud structures, which leads to an underestimation of liquid water
75 mass mixing ratio (Storelvmo et al., 2008; Tan & Storelvmo, 2016; Zhang M. et al., 2019). In
76 addition, the interaction between cloud microphysics and other physical processes (e.g., shallow
77 convection) has also been found to play an important role in modeled mixed-phase cloud
78 properties. For example, the detrainment of liquid from shallow convection to stratiform clouds
79 increases the amount of cloud liquid water in simulated mixed-phase clouds over the Southern
80 Ocean. This leads to a large reduction of the surface shortwave radiative fluxes over that region
81 as demonstrated in the Community Atmosphere Model version 5 (CAM5) (Kay et al., 2016;
82 Wang et al., 2018).

83 The mixed-phase cloud properties simulated by the newly developed U.S. Department of
84 Energy (DOE) state-of-the-art GCM, Energy Exascale Earth System Model (E3SM, Golaz et al.
85 2019) atmosphere model version 1 (EAMv1) (Rasch et al., 2019; Xie et al., 2018) have shown a

substantial change from the EAMv1 predecessor, CAM5. In particular, EAMv1 is found to have too large liquid phase cloud fraction and a moderate underestimation of ice phase cloud fraction between -20℃ and -30℃ over the high-latitudes in both hemispheres (Zhang Y. et al., 2019). This is different from what is found in Kay et al. (2016), which showed that CAM5 had insufficient supercooled liquid clouds. The EAMv1 simulated mixed-phase cloud supercooled liquid fraction (SLF), which is defined as the ratio of liquid water mass to total condensed water mass, is significantly larger than in CAM5 over the Southern Ocean for temperatures colder than -13℃. This leads to smaller biases in shortwave cloud radiative effect when comparing to the observation (Rasch et al., 2019). The increased supercooled liquid in EAMv1 is partially related to the reduced WBF process rate that has been artificially slowed down by 10 times through a tuning parameter compared to CAM5. In a sensitivity test, Zhang Y et al. (2019) showed that the EAMv1 simulated SLF is still much larger than that produced by CAM5 even after the tuning of the WBF process was eliminated. This indicates that other changes in model physics made in the development of EAMv1 from CAM5 also play an important role in the increased SLF in simulated mixed-phase clouds.

As described in Xie et al. (2018), there are three major changes in model physics associated with mixed-phase clouds made during the development of EAMv1 from CAM5. First, EAMv1 adopts the CNT ice nucleation scheme to replace the previous temperature dependent heterogeneous ice nucleation scheme (Meyers et al., 1992) used in CAM5 in mixed-phase cloud regime. As shown in Wang et al. (2018), this change leads to a large increase in SLF at the temperatures colder than -20℃ in the polar regions because the Meyers scheme predicts much higher INP number concentrations than CNT (Liu et al., 2011; Xie et al., 2013) in clean

environments. This may cause the model to significantly overestimate INP number concentrations compared to observations (Prenni et al., 2007). Second, EAMv1 uses a simplified third-order turbulence closure parameterization (CLUBB) (Golaz et al., 2002; Larson, 2017; Larson & Golaz, 2005) that unifies the treatment of planetary boundary layer (PBL) turbulence, shallow convection, and cloud macrophysics to remove the unrealistic separation of these physical processes, which are the characteristics of most climate models including CAM5. This will impact the detrainment of cloud water from shallow convection to stratiform clouds, which in turn affects the simulated mixed-phase clouds. Meanwhile, the CLUBB has been found to explain the improvements in EAMv1 simulated cloud climatology. These improvements include the increased cloud fraction of low-level stratocumulus (Sc) and trade wind cumulus (Cu) near the subtropical coasts, and the better transition from Sc to Cu, compared to CAM5 (Xie et al., 2018). Third, the last major relevant change is to use the second version of the two-moment cloud microphysical scheme, MG2 (Gettelman & Morrison, 2015). The new scheme predicts the mass and number mixing ratios of snow and rain hydrometeors instead of the diagnostic treatment applied in its first version (MG1, Morrison & Gettelman, 2008). The collection of liquid droplets by rain drops through the accretion process tends to become more dominant than autoconversion, which is more comparable to the cloud-resolving model simulations (Gettelman et al., 2015).

The goal of this study is to provide a process-level understanding on how these changes, which were made to improve cloud physical processes during the EAMv1 development, impact the model simulated high-latitude single-layer mixed-phase clouds in the Arctic. This is done through well-designed sensitivity experiments, which are conducted by utilizing the short-term

hindcast framework developed by the DOE Cloud-Associated Parameterizations Testbed (CAPT) project (Ma et al., 2015; Phillips et al., 2004). Under the CAPT framework, a climate model is initialized with realistic conditions from Numerical Weather Prediction (NWP) center analysis, and its representation of atmospheric physical processes is tested in short-range weather forecasts. As there are no real-time operational constraints, retrospective forecasts (hindcasts) are performed. The rationales behind this approach are: (1) the large-scale state of the atmosphere in the early periods of a forecast is realistic enough that errors can be ascribed to the parameterizations of atmospheric processes; and (2) atmospheric physical processes (e.g., moist process) are often fast (~hours) and the large-scale state changes more slowly (~days). As indicated in earlier studies (Ma et al., 2014; Williams & Brooks, 2008; Xie et al., 2012), there is a strong correspondence between short- and long-term systematic errors in climate models, particularly for those fields that are related to fast physics (e.g., clouds). Most systematic errors are apparent in day 2 hindcasts. These errors steadily grow with the hindcast lead time and typically saturate after five days with amplitudes comparable to the climate errors. Using initialized climate models for testing physical parameterizations allows for evaluation of the nature of parameterization errors before longer-time scale feedbacks develop, and thus provides essential clues to the origin of climate errors (Liu et al., 2011; Xie et al., 2008; Zheng et al., 2016). It facilitates process studies by directly linking model deficiencies to atmospheric processes through case studies using data collected from field campaigns. In this study the observations collected from the ARM Mixed-Phase Arctic Cloud Experiment (M-PACE) field campaign (Verlinde et al., 2007), which was conducted at the ARM North Slope of Alaska (NSA) site during October 2004, are used to evaluate the EAMv1 simulated mixed-phase clouds.

This paper is organized as follows. Section 2 provides the details about EAMv1, particularly its parameterizations related to mixed-phase clouds, model experiments, and observation data used in this study. Section 3 discusses the simulated mixed-phase clouds and their microphysical properties. Section 4 presents a detailed process analysis. Conclusions and discussions are given in Section 5.

2. Model, model experiments, and observation data

2.1. EAMv1

EAMv1 is developed from CAM5 with a significant increase of model resolution and notable changes to its physical parameterizations (Rasch et al., 2019; Xie et al., 2018). It can be run at either 1 degree or 0.25 degree in horizontal and 72 layers in vertical with the model top extended to ~60 km. Within the PBL, 17 vertical layers are included below 1.5 km with the vertical resolution from 20 m to 200 m.

The updated physics includes using CLUBB for a unified treatment of PBL turbulence, shallow convection, and cloud macrophysics. These processes were represented by the University of Washington (UW) PBL turbulence scheme (Bretherton & Park, 2009), shallow convection scheme (Park & Bretherton, 2009), and cloud macrophysics scheme (Park et al., 2014) in CAM5. CLUBB achieves the high-order closure through a set of triple joint probability density function (PDF) of vertical velocity (w), liquid water potential temperature (θ_l), and total specific water content (q_t). A double Gaussian function is assumed to define the shape of trivariate PDF. CLUBB predicts the variances of and correlations between θ_l, q_t, and w, as well

as the third moment $\overline{w'^3}$ to determine the parameters of the assumed joint PDF. Momentum terms such as $\overline{u'^2}$, $\overline{v'^2}$ are also prognostically determined in CLUBB, while other momentum terms such as $\overline{u'w'}$, $\overline{v'w'}$ are determined diagnostically and closed using a down-gradient approach as described in Golaz et al. (2002). Once the joint PDF is known, other higher-order moments (turbulent advection terms such as $\overline{w'^2 q_t'}$, $\overline{w' q_t'^2}$, $\overline{w' \theta_l'^2}$) can be closed by integrating over the assumed PDF to achieve the closure in CLUBB prognostic equations. Cloud quantities such as the cloud fraction and cloud liquid water mixing ratio can be diagnosed directly via the integration of the joint PDF over the saturated portion (Larson et al., 2002). We note that the current CLUBB scheme is designed for liquid-phase processes. Only the transport of cloud ice mass mixing ratio is treated via a turbulence eddy diffusion scheme (Bogenschutz et al., 2013). Ice-phase processes are not explicitly included in the CLUBB's PDF approach but are treated via cloud microphysics. The ice cloud fraction is determined based on relative humidity when using CLUBB (Gettelman et al., 2010).

CLUBB is paired with the same deep convection scheme used in CAM5 (i.e., the ZM scheme developed by Zhang & McFarlane, 1995) and the updated cloud microphysical scheme MG2. MG2 prognoses the mass and number concentrations of cloud liquid and ice and precipitating hydrometeors (snow and rain). The reduction in number concentrations of precipitating hydrometeors due to evaporation is also accounted for in the prognostic treatment. To better couple with the CLUBB parameterization, sub-time steps of 5 min are used in the cloud microphysics. Compared to the MG1 microphysics, MG2 updates the number concentration of prognostic cloud droplets due to activation at the beginning of the cloud microphysics scheme. Furthermore, the CNT ice nucleation scheme is adopted to represent the

immersion, contact, and deposition heterogenous freezing in the mixed-phase cloud regime (Wang et al., 2014). CNT links the ice particle formation to aerosol (i.e., dust and soot) properties such as aerosol number concentration and particle size (Hoose et al., 2010). Other major updates include the 4-mode version of the Modal Aerosol Module (MAM4) (Liu et al., 2016), the unified treatment for convective transport and scavenging of aerosols (Wang et al., 2013), the resuspension of aerosol particles from evaporated raindrops to coarse mode, the representation of marine organic aerosols, and a linearized ozone chemistry (Linoz2) mechanism (Hsu & Prather, 2009; McLinden et al., 2000) for representing stratospheric ozone and its radiative effects in the stratosphere.

As indicated in Xie et al. (2018), EAMv1 is quite sensitive to the changes made in physics and model resolution. To obtain a reasonable TOA energy flux and optimize the model performance, substantial model re-tuning was performed during the EAMv1 development. The model tuning has emphasized on exploring simulation sensitivity to a few loosely constrained parameters used in the model parameterizations (e.g., CLUBB, ZM, and MG2), guided by using the perturbed-physics ensemble method as described in Qian et al. (2018) and Zhang et al. (2012), with the goal to identify a model configuration that yields the best simulation against observations while keeps the TOA energy budget balanced to avoid a drift of climate. The tuning was made primarily to those parameters that have major impacts on the simulations of clouds and precipitation, in particular over the tropical and subtropical regions. Mixed-phase clouds at high latitudes were not the target for the tuning. More details about the changes made in turbulence, cloud, and convection related parameterizations and model tuning are provided in Xie et al. (2018).

2.2. Model experiments

Table 1 lists the model experiments conducted in this study. The control experiment ("CTL") has the same model configuration as the default low resolution EAMv1, except that we remove the artificial parameter that is applied to the WBF process. This is also the case for all other sensitivity experiments. In this way, we can exclude the impact of changes in the WBF process on the model simulated Arctic mixed-phase clouds.

Three sensitivity tests are performed in this study. In "MEYERS", the CNT scheme in CTL is replaced by the Meyers et al. (1992) scheme. As the number concentration of nucleated ice particles differs largely between these two schemes, this experiment is designed to understand the influence of heterogeneous ice nucleation on the partitioning of cloud condense. In "UW", CLUBB in CTL is replaced by the UW schemes for PBL turbulence, shallow convection and cloud macrophysics that were used in CAM5, to test the role of CLUBB on the simulated cloud properties. Finally, in "UW_MG1" which is based on the "UW", MG2 is replaced by MG1 to test the impact of the MG2 microphysics. We note that we use EAMv1 as the baseline, because we want to trace back reasons for the model behavior change during the EAMv1 development of physical parameterizations. EAMv1 provides the option for users to switch back to certain old parameterizations without too much effort.

For each experiment, a series of 3-day hindcasts (Ma et al., 2015) are initialized every day from 30 September 2004 to 31 October 2004 to cover the M-PACE period. The initial conditions of the large-scale states (i.e., horizontal wind, temperature, and water vapor) are from the European Centre for Medium-Range Weather Forecasts (ECMWF) ERA-Interim reanalysis

239 (Dee et al., 2011). Since the model is initialized from a foreign model data assimilation system,
240 and to avoid potential problems in the model spin-up, we skip day 1 (0 – 24 hr) hindcasts and use
241 day 2 (24 – 48 hr) hindcasts in the analysis (Ma et al., 2013, 2014). The large-scale state in the
242 day 2 hindcasts is still close to the initial state so that we can focus on deficiencies in model
243 parameterizations. To compare with the ARM M-PACE observations, model outputs at the land
244 grid point closest to the ARM NSA Utqiaġvik site (71.3°N, 156.6°W) are extracted. We note that
245 using "nudging" instead of "the short-term forecasts" is another way to facilitate the comparison
246 to field data (Zhang et al., 2014). In the nudging approach, the model states are continuously
247 nudged toward reanalysis to ensure realism. However, nudging limits the freedom for model
248 errors to grow.
249
250 **2.3. M-PACE observations**
251 Table 2 summarizes the observational data used for model evaluation in this study. The
252 cloud microphysical properties were retrieved using different algorithms as summarized in the
253 ARM cloud retrieval ensemble dataset (ACRED) (Zhao et al., 2012). ACRED provides a rough
254 estimate of uncertainties in derived cloud microphysical properties that are attributed to the
255 retrieval techniques. For M-PACE, five different retrieval products are available, which are
256 either from the ARM baseline retrievals (MICROBASE) or from individual research groups. At
257 the NSA site, four products are available for liquid water (MICROBASE, SHUPE_TURNER,
258 WANG, and DONG) while ice water retrievals contain three different methods (MICROBASE,
259 SHUPE_TURNER and WANG) (Zhao et al., 2012). MICROBASE is the ARM baseline cloud
260 retrieval product. Different from other physically-based methods, MICROBASE utilizes an

empirical parameterization to retrieve liquid water content (LWC) (Frisch et al., 1995; Liao & Sassen, 1994) and ice water content (IWC) (Ivanova et al., 2001; Liu & Illingworth, 2001) in mixed-phase clouds. SHUPE_TURNER adopts both physically-based and empirical methods to retrieve mixed-phase cloud properties. For liquid phase, Turner (2005) is used for thin clouds, and Frisch et al. (1995) used for pure liquid clouds. Ice phase properties are retrieved utilizing the method of Shupe et al. (2005). Algorithms used in the WANG product are designed specifically for mixed-phase clouds. Both radar and lidar measurements are combined to retrieve the cloud properties (Wang et al., 2004; Wang & Sassen, 2002). Last, the DONG product only includes cloud properties in the liquid phase, with LWP retrieved based on the microwave radiometer (MWR) and millimeter-wavelength cloud radar (MMCR) measurements following Dong and Mace (2003). More details can be found in Zhao et al. (2012). The hourly-averaged ACRED data in October 2004 is used for validating the short-term hindcast results.

Other observational data used in this study include the frequency of cloud occurrence based on the integrated measurements from ARM cloud radars, lidars, and laser ceilometers with the Active Remotely Sensed Clouds Locations (ARSCL) algorithm (Clothiaux et al., 2000). In-situ measurements of the microphysical properties of single-layer boundary layer mixed-phase clouds between 9 - 12 October 2004 (McFarquhar et al., 2007) are also used. During this period, four flights were conducted with the University of North Dakota (UND) Citation aircraft. Each flight lasted for 1 - 2 hours with cloud data collected every 10s.

3. Results

3.1. Modeled mixed-phase clouds

Large-scale synoptic circulation played an important role in the formation and maintenance of clouds during the M-PACE field campaign (Verlinde et al., 2007; Xie et al., 2006). A high-pressure system was developed to the northeast of the Alaska coast in the early period of the experiment (5 - 14 October). The east-northeasterly flow prevailed over the NSA site in the lower troposphere. Cold air associated with the cold pack ice to the north of Alaska reached the NSA. Together with a weak trough in the upper level, surface temperature dropped considerably below -10℃ by 8 October. From 9 to 14 October, resilient single-layer boundary layer mixed-phase clouds formed over the open ocean and were advected to the NSA site (Figure 1a). Weak updrafts (~ 0.5 m/s) were associated with these clouds. After 14 October, the surface high-pressure system slowly propagated southeastward, and a strong low-pressure center that formed near Kamchatka began to influence Alaskan coasts, which brought southerly and southwesterly flow to the NSA. Deep clouds were frequently observed during this time period, associated with frontal systems generated by this low.

Figure 1 compares the time-pressure cross section of ARM observed cloud frequency of occurrence and modeled grid-mean cloud fraction from the day-2 hindcasts at the NSA Utqiaġvik site. Note that the single-layer low-level mixed-phase clouds from 9 to 14 October are typical and ubiquitous over the Arctic region. In the following discussion, we will focus our analysis on this type of clouds, to understand how changes of EAMv1 physical parameterizations affect their simulation. Compared with the ARSCL observation (Figure 1a), CTL well simulates the resilient low-level mixed-phase clouds between 9 - 14 October (Figure 1b). Cloud temporal

303 evolution as well as the cloud top height are captured by the model. Simulated cloud base,
304 however, is slightly lower than the observation. We note that the cloud base (top) is defined as
305 the lowest (highest) level with non-zero cloud fraction simulated in the model.

306 In general, simulated maximum cloud fraction shows little sensitivity to the
307 parameterization change during the examined time period (Figures 1c, 1d, and 1e). In contrast,
308 simulated cloud boundary is quite sensitive to the examined parameterizations. For example, the
309 change of ice nucleation scheme from the Meyers to CNT, leads to an increased cloud base
310 height and cloud top height, closer to the observations (Figure 1c). Using CLUBB to replace the
311 UW schemes, however, results in a lower cloud base height and cloud top height (Figure 1d).
312 Because cloud fraction is determined via the relative humidity in the UW cloud macrophysics
313 scheme (Park et al., 2014), the clearer separation between cloud base and surface below 950 hPa
314 in UW is mostly attributed to the drier atmosphere near the surface, while more moisture near the
315 cloud top is responsible for the higher cloud top in UW (not shown). Compared to MG1, the
316 MG2 microphysics parameterization improves cloud base height as indicated in Figure 1e. Cloud
317 top also becomes higher with the use of MG2 microphysics. Note that the pattern with noisier
318 cloud base in UW and UW_MG1 may be the result of total consumption of liquid water in the
319 lower portion of clouds, which will be discussed later.

320 Although the overall cloud structure is reasonably produced for the single-layer mixed-
321 phase clouds, large impacts from different model schemes are found on the simulated liquid
322 water and ice water mass mixing ratios. Figure 2 shows the modeled LWC, IWC, and SLF in the
323 CTL and three sensitivity experiments. Note that rain and snow water mass mixing ratios are
324 added to LWC and IWC, respectively, to better compare with ground-based observations which

cannot distinguish them. One unexpected result shown in Figure 2 is that CTL simulates almost no ice water mass mixing ratio during 9 - 14 October. Supercooled liquid water constitutes nearly all the cloud condensate mass mixing ratio, at temperatures about -14℃, in the single-layer low-level mixed-phase clouds (Figures 2a and 2e). SLF is therefore close to 1 for these clouds (Figure 2i). This model behavior is in contrast to previous M-PACE studies with CAM5, where cloud ice water was commonly overestimated, and cloud liquid water was substantially underestimated (Liu et al., 2011; Xie et al., 2008, 2013). Since the artificial tuning parameter for the WBF process is removed in CTL, the significant underestimation of IWC is most likely a result of too little ice being produced in the single-layer mixed-phase clouds. More discussion will be provided later.

Compared to CTL, more IWC is produced in MEYERS, which indicates that the use of CNT leads to lower simulated IWC in single-layer mixed-phase clouds. This can be explained by the fact that CNT produces four orders of magnitude lower number concentration of INPs than MEYERS at temperatures ~ -15℃ (figure not shown). Consistent with earlier studies, Shi and Liu (2019) found that CNT tends to generate lower INP number concentration than observations at warm temperatures, while the Meyers scheme overestimates observed INP number concentrations (DeMott et al., 2010). The use of CLUBB also plays an important role in the decrease of cloud ice, as seen by comparing CTL and UW (Figures 2e and 2g). MG2 microphysics slightly reduces IWC and increases LWC when comparing UW to UW_MG1 (Figures 2c and 2g with Figures 2d and 2h). Even though the sequence of updating the number concentration of cloud droplets due to activation is changed in MG2, the difference between UW and UW_MG1 is mainly due to the higher accretion rate of cloud liquid by rain. The conversion

347 from cloud liquid to ice becomes weaker as more liquid is collected by rain drops. Moreover,
348 compared to CTL, UW_MG1 substantially decreases LWC, and increases IWC in the modeled
349 single-layer mixed-phase clouds. Despite the use of CNT in the UW_MG1 experiment, the
350 partitioning pattern between LWC and IWC in UW_MG1 is similar to what was shown in
351 CAM5 (Liu et al., 2011; Xie et al., 2013). When the Meyers ice nucleation scheme is used in
352 UW_MG1, more IWC and less LWC are produced (not shown), making UW_MG1 more
353 comparable to CAM5. Nevertheless, the similarity between UW_MG1 (using either Meyers
354 scheme or CNT scheme) and CAM5 demonstrates that changes of model dynamic core, vertical
355 and horizontal resolutions, and model tuning are not the important reasons for the largely
356 underestimated IWC in this single-layer mixed-phase cloud case.

357 Figure 2 also shows the time-pressure cross sections of SLF for modeled mixed-phase
358 clouds. It is shown that the distribution of high SLF (close to 1) corresponds well with that of
359 LWC. Less spatial occurrence of high SLF is simulated when Meyers ice nucleation, UW
360 schemes, and MG1 cloud microphysics are utilized.

361 Consistent with the lack of total cloud ice mass mixing ratio, a very low number
362 concentration ($< 0.01\ L^{-1}$) of cloud ice particles is produced in CTL between 9 - 14 October,
363 particularly at temperatures between -10℃ and -15℃, within the single-layer boundary layer
364 mixed-phase clouds (Figure 3). It is clear that the three updated physical parameterizations
365 during the EAMv1 development tend to decrease the ice particle number concentration as shown
366 in Figures 3b-3d. Substantially more ice crystals are produced after replacing the new schemes
367 (i.e., CNT, CLUBB, and MG2) with the old ones (i.e., Meyers, UW, and MG1). Comparing
368 these three parameterizations, uses of CLUBB and MG2 have stronger impacts than CNT.

Figure 4 compares modeled LWP and IWP to various retrievals contained in the ARM ACRED data product. In general, differences are smaller among liquid phase retrievals compared to those of ice phase retrievals. One to two orders of magnitude difference can be found in IWP products, which could be the result of assumptions made in different algorithms (Zhao et al., 2012). For example, assumptions about size distribution, shape, and density of ice crystals can vary substantially, contributing to large uncertainties in IWP retrievals. Compared to the ground-based observations, CTL overpredicts LWP during more than half of the time from 10 to 13 October. Meanwhile, CTL underestimates the observed IWP by 3 - 5 orders of magnitude during 9 - 14 October. When comparing sensitivity experiments to CTL, we note that less LWP and more IWP are simulated given a particular suite of parameterizations.

Figure 5 shows the comparison of SLF as a function of normalized cloud height between in-situ measurements from the UND Citation aircraft and the EAM hindcast experiments. Aircraft data were processed by McFarquhar et al. (2007). Note that cloud altitude is normalized from 0 at cloud base to 1 at cloud top for both the observations and model results. Modeled clouds are defined when total cloud water mass mixing ratios are larger than 0.001 g kg^{-1}. The in-situ measurements were obtained on 9, 10, and 12 October during the M-PACE field campaign, to capture the vertical structures of single-layer mixed-phase clouds and their microphysical properties (e.g., LWC and IWC). There were two flights on 9 October, and one flight on 10 and 12 October, respectively. In Figure 5, data from the two flights on 9 October are combined with the same color.

The aircraft measurements (Figure 5a) show that the observed SLF increases with normalized cloud height and is larger than 80% near the cloud top. Larger fraction of cloud ice is

391 observed in the lower portion of clouds, indicated by the lower SLF near the cloud base. The
392 vertical distribution of SLF is similar among the four research flights. Consistent with earlier
393 discussion, Figure 5b shows that CTL substantially overestimates SLF within the single-layer
394 mixed-phase clouds. Simulated SLF remains close to 100% for all cloud layers during the
395 examined period. Compared to CTL, MEYERS better reproduces the vertical distribution of SLF
396 in observations, but its SLF near the cloud base is underestimated. In addition to the fact that
397 cloud ice water mass mixing ratio is included in our definition of cloud base, the underestimated
398 SLF can also be explained by the overestimated INP number concentration by the Meyers
399 scheme near the cloud base. Higher number concentration of ice particles and larger ice water
400 content are generated near the surface in MEYERS than CTL, as shown in earlier figures. It is
401 clearly shown in Figure 2b and 2f that cloud liquid water tends to distribute separately from
402 cloud ice water in modeled clouds. Figure 5d shows that the feature of SLF increasing with
403 normalized cloud height is captured by the UW schemes on 10 and 12 October, while such trend
404 is poorly simulated on 9 October. Too much cloud ice water is simulated near the cloud base in
405 UW on 9 October. We note that 9 October is a transition period in terms of the large-scale
406 synoptic conditions during the M-PACE campaign. A high-pressure system was built over the
407 pack ice to the northeast direction of Alaskan coast and brought cooled air to the Utqiaġvik site,
408 decreasing surface temperature by ~5℃ during 9 October (Verlinde et al., 2007). The different
409 SLF patterns between 9 October and 10 and 12 October shown in Figure 5d may be explained by
410 the inadequate representation of this transition in the UW schemes. In contrast to UW,
411 UW_MG1, in which MG2 is replaced by MG1, does not show the inclining SLF along the

412 normalized cloud height on 10 and 12 October, indicating that the use of MG2 microphysics is
413 able to improve the SLF vertical distribution of modeled single-layer mixed-phase clouds.

414

415 **4. Mass budget analysis**

416 In this section we further analyze detailed cloud microphysical budgets for the four
417 hydrometeors -- cloud liquid, cloud ice, rain, and snow -- for the single-layer mixed-phase clouds
418 during the period between 9 - 11 October. The purpose is to understand which cloud
419 microphysical process is most important to model behavior changes. The budget terms of
420 microphysical process tendencies are vertically integrated over the whole cloud layers and are
421 averaged over the selected time period.

422 A more detailed discussion of how different physical parameterizations in EAMv1
423 interact with each other is provided in Figure 1 of Zhang et al. (2018). In this section, we will
424 only focus on the impacts of shallow convection, cloud macrophysics, ice nucleation, and cloud
425 microphysics as well as their interactions on simulated mixed-phase cloud properties. In EAMv1,
426 CLUBB (or shallow convection scheme and cloud macrophysics in the UW schemes), ice
427 nucleation, and cloud microphysics are updated subsequently. Calculated physical process rates
428 are used to update the quantities of cloud properties before passing them to the next
429 parameterization. Therefore, the calculation sequence of physical processes is important when
430 interpreting the following discussion.

431

432 **4.1. Impact of heterogeneous ice nucleation**

Figure 6a shows that liquid water condensation constitutes the major source for cloud liquid condensate in both CTL and MEYERS. Note that the amount of condensed liquid water is directly diagnosed from the assumed joint PDF in the CLUBB parameterization (Bogenschutz et al., 2012; Golaz et al., 2002). Although four orders of magnitude difference are found in the number concentration of nucleated ice particles between CTL and MEYERS (figure not shown), comparable liquid condensation tendencies are found in both experiments. This is expected, as different heterogeneous ice nucleation schemes should have minimal impacts on the liquid water formation.

With a small amount of total ice mass mixing ratio produced in the single-layer mixed-phase clouds between 9 and 11 October in CTL, ice phase associated microphysical processes are active at limited rates. For instance, the WBF process with respect to ice and snow, and the snow accretion of liquid droplets are weakly activated to transfer formed liquid water to ice and snow. However, almost all the generated cloud ice water is converted to snow via autoconversion (Figure 6c). Snow water then tends to sediment out of clouds, leaving negligible amount of total ice water mass mixing ratio in CTL simulated mixed-phase clouds. Comparing MEYERS to CTL, with a higher ice particle number concentration from the heterogeneous ice production, larger tendencies of ice associated processes are shown in MEYERS. In particular, the WBF process rate with respect to ice is much increased, which leads to a larger cloud ice mass mixing ratio. As the growth of snow water mass mixing ratio is strongly influenced by the autoconversion of cloud ice, larger snow growth rates such as the WBF process with respect to snow, and snow accretion of liquid droplets are shown in Figure 6d in MEYERS. Meanwhile, the different ice number concentration also changes the pathway of whether liquid droplets are

455 collected by rain drops or snow particles. For example, when higher ice number concentration is
456 formed by MEYERS, more liquid droplets are collected by snow, inhibiting the accretion of
457 liquid droplets by rain drops (Figure 6b). This further increases the ratio of total ice water mass
458 mixing ratio to total liquid water mass mixing ratio. Therefore, the number concentration of ice
459 particles generated from heterogeneous ice nucleation is important for the Arctic single-layer
460 mixed-phase clouds. Ice production from the CNT scheme in CTL is too weak at temperatures
461 warmer than -15℃. We note that the impact of heterogeneous ice nucleation on simulated mixed-
462 phase clouds is important more through its influence on cloud ice number concentration, not on
463 ice mass mixing ratio. As shown in Figure 6a, the mass tendency for heterogeneous ice
464 nucleation is substantially small. This is because the mass of newly formed ice crystals is so
465 small that ice nucleation cannot have a comparable mass tendency to other processes such as the
466 WBF process. However, this does not impair the importance of heterogeneous ice nucleation, as
467 cloud ice mass growth rate depends sensitively on the number concentration of ice particles.

468

469 **4.2. Impact of CLUBB**

470 Comparing UW to CTL, the change of physical processes due to the use of CLUBB can
471 be analyzed. In the UW experiment, liquid condensation is determined by cloud macrophysics
472 (Park et al., 2014), and the shallow convection is calculated by Park and Bretherton (2009).
473 When shallow convection is separately treated in the UW parameterization, liquid mass mixing
474 ratio detrained from shallow convection is of comparable magnitude to the condensation (Figure
475 6a). However, the detrainment and condensation processes cannot be diagnosed separately in

476 CTL, since CLUBB implicitly calculates the total production of cloud liquid water via the
477 integral over saturated portion of the joint PDF (Golaz et al., 2002; Larson et al., 2002).

478 Similar to the cloud liquid water mass budget, detrainment from shallow convection also
479 constitutes the source for cloud ice mass mixing ratio when CLUBB is not used (Figure 6c).
480 Such detrained cloud ice particles, together with the nucleated ice particles from heterogeneous
481 ice nucleation, participate in the cloud ice mass growth. We emphasize here the importance of
482 initial cloud ice amount (either from the shallow convection detrainment or from the
483 heterogeneous ice nucleation), because one prerequisite for cloud ice mass growth is that
484 sufficient ice particles exist at the beginning of cloud microphysics calculation. As noted in
485 section 2.1, ice phase related processes are currently not explicitly treated in the CLUBB's PDF
486 method. Instead, only the transport of cloud ice mass mixing ratio is treated in CLUBB through
487 an eddy diffusion scheme. However, the eddy diffusion transport is found to be inactive in the
488 examined low-level boundary layer mixed-phase clouds (shown as CLUBB process in Figure
489 6c). Compared to UW, without initial ice from the shallow convection when CLUBB is used, the
490 increase of cloud ice mass mixing ratio by subsequent cloud microphysical processes becomes
491 substantially weaker in CTL. Example includes the lower WBF process tendency with respect to
492 ice.

493 Meanwhile, it is shown in Figure 6c that the growth of ice crystals through water vapor
494 deposition also contributes to the cloud ice mass mixing ratio in UW, but this source is not
495 evident in CTL. In the MG cloud microphysical scheme, ice depositional growth is
496 parameterized as two separate processes: the WBF process and ice deposition at the expense of
497 water vapor. The WBF process represents the conversion of cloud liquid to ice (and snow),

assuming homogeneous mixing between liquid and ice (and snow) in each grid cell at subfreezing temperatures. Since the MG scheme does not treat the evaporation of cloud liquid water, the evaporation of liquid droplets in the WBF process is not numerically represented. When abundant cloud ice coexists with cloud liquid in mixed-phase clouds, the WBF process will first consume the available liquid water. Under the circumstance that cloud liquid water is totally consumed within one model time step (5 minutes, as sub-step is used in cloud microphysics), ice crystals will then continue their growth at the expense of water vapor until the end of that sub-step. The latter process is referred to as ice depositional growth in the MG scheme. Therefore, the indication of ice deposition in UW implies that all available liquid water in simulated clouds is completely consumed at certain levels or at certain time steps, but such complete consumption never occurs in CTL. Furthermore, because of the larger source for cloud ice mass mixing ratio in UW, snow water also becomes more abundant via autoconversion of cloud ice. Accretion of liquid and rain by snow particles is enhanced, which further increases the amount of ice phase cloud condensates.

Therefore, in CTL modeled single-layer low-level mixed-phase clouds, CLUBB parameterization substantially underestimates one source of cloud ice water that is represented in Park and Bretherton (2009). As a result, the lack of initial cloud ice amount substantially reduces the ice mass growth through subsequent microphysical processes, leading to the underestimation of total ice mass mixing ratio.

4.3. Impact of MG2

519 The impact of cloud microphysical parameterization change from MG1 to MG2 can be
520 examined by comparing UW and UW_MG1 experiments. The use of MG2 reduces the process
521 tendencies for ice and snow growth at the expense of cloud liquid water. For example, the WBF
522 process with respect to both ice and snow, as well as the snow accretion of liquid droplets
523 become weaker in UW than UW_MG1. It is noted that the change in the sequence of updating
524 activated droplet number concentration in MG2 has insignificant impact on our examined Arctic
525 single-layer mixed-phase clouds (not shown). Thus, these changes of process tendencies are
526 attributed to the prognostic treatment of precipitation hydrometeors (rain and snow) in the MG2
527 microphysics. Another important aspect in MG2 simulated mixed-phase clouds lies in the higher
528 accretion rate of liquid droplets by rain drops as shown in Figure 6a and 6b. Although the total
529 cloud ice mass mixing ratio is reduced in MG2 simulated mixed-phase clouds, there is no
530 significant change in the formation of initial cloud ice. For example, the heterogeneous ice
531 nucleation is the same between UW and UW_MG1. The detrained cloud ice from shallow
532 convection also behaves similarly. Therefore, the change of cloud microphysics should not be as
533 important as the other two parameterizations. Nevertheless, as noted in Gettelman et al. (2014),
534 MG2 simulated mixed-phase clouds are strongly sensitive to the ice particle number
535 concentration. The change of initial ice source can then have a stronger impact on the cloud
536 microphysical processes in MG2 than MG1.

537

538 **5. Summary and discussions**

539 In this study, we utilize the short-term hindcast approach to understand which physical
540 process is most responsible for the significant behavior change in Arctic single-layer mixed-
541 phase clouds simulated by the U.S. DOE E3SM atmospheric model (EAMv1), compared to its
542 predecessor, CAM5. Hindcast results show that the amount of total ice water mass mixing ratio
543 is substantially underestimated in the default EAMv1, particularly for the single-layer boundary
544 layer mixed-phase clouds during the M-PACE. On the other hand, total liquid water mass mixing
545 ratio is overestimated when compared with the ARM ground-based remote sensing data. By
546 tracing back the changes made in EAMv1, we find that uses of the CNT scheme, CLUBB
547 parameterization, and MG2 microphysics all tend to decrease ice mass mixing ratio. When all
548 three schemes are combined, the decrease of ice mass mixing ratio resulting from individual
549 scheme change tends to add up, leading to a large underestimation of ice water amount in
550 modeled clouds. A detailed budget analysis of cloud microphysical process tendencies indicates
551 that the initial ice particles, generated from heterogenous ice nucleation and detrainment of cloud
552 ice from shallow convection, are critical for the ice mass increase through subsequent cloud
553 microphysical processes. When CNT and CLUBB are used to respectively replace the Meyers
554 ice nucleation scheme and the UW schemes, a minimal number of initial ice particles are
555 generated and passed to cloud microphysics. As the mass growth rate of ice crystals depends
556 sensitively on the number concentration of ice particles, simulated cloud ice mass mixing ratio is
557 then reduced. For example, the WBF process with respect to ice is much weaker in CTL
558 compared to the three sensitivity experiments. In addition, the formation of snow water is also
559 reduced in CTL, which leads to a weaker collection of liquid droplets, rain drops, and ice
560 particles by snow. Since MG2 microphysics scheme does not impact the initial ice crystals,

561 change in microphysics should not be a primary reason for the underestimation of cloud ice.
562 However, the introduction of MG2 reduces the WBF process with respect to both ice and snow,
563 as well as the snow accretion of liquid droplets, which also results in lower total ice mass mixing
564 ratio.

565 Along with the change from UW to CLUBB, the treatment of PBL turbulence is also
566 changed. We notice changes in the simulated PBL. For example, the vertical updraft and
567 potential temperature profiles produced from CLUBB and UW scheme are different. However,
568 the difference is not substantial. Therefore, the PBL change may not be an important factor to
569 influence the phase partitioning of mixed-phase clouds in this study.

570 We note that the issue analyzed in this study is mostly related to the Arctic single-layer
571 boundary layer mixed-phase clouds. In particular, the insufficient ice formation from the CNT
572 heterogeneous ice production is more problematic for mixed-phase clouds at temperatures
573 warmer than -15℃. With the CNT ice nucleation linked to aerosol properties, the model
574 deficiency in aerosol fields can influence modeled mixed-phase clouds. EAMv1, like many other
575 GCMs, underestimates the dust transport from mid-latitude sources, misses the Arctic local dust
576 sources, and neglects biological aerosols. This leads to the substantial underestimation of INP
577 number concentrations over the Arctic region (Shi & Liu, 2019). Such biases in modeled
578 aerosols and INPs contribute to the biased phase partitioning of high latitude mixed-phase clouds
579 in EAMv1. Future model development should focus on the treatment of aerosol emission and
580 scavenging processes to obtain accurate aerosol concentrations and distributions in the
581 atmosphere. In addition to the CNT scheme, other advanced ice nucleation parameterizations
582 also determine INP number concentrations based on aerosol properties. For example, DeMott et

583 al. (2015) parameterization determines INP number concentration based on temperature and
584 number concentration of dust particles with sizes larger than 0.5 μm in diameter. Niemand et al.
585 (2012) links the INP concentration to the surface area of dust particles and temperature.
586 Therefore, biases in the aerosol simulation will affect the modeled ice nucleation due to aerosol-
587 cloud interactions. To address the issue in CLUBB parameterization, a similar approach from
588 Park and Bretherton (2009) to partition condensed cloud water may help. Ice phase should also
589 be considered in CLUBB's PDF parameterization in order to develop a unified framework for
590 shallow convection, PBL turbulence, and cloud macrophysics for mixed-phase clouds.
591 Moreover, other cloud microphysical processes, which are important for increasing cloud ice
592 mass or number concentration, may not be reasonably parameterized in current microphysics
593 scheme. For example, the secondary ice production is not well represented in current GCMs
594 (Field et al., 2017).

595 Although this study is based on an analysis of the M-PACE field campaign at one single
596 location, the overly dominated cloud liquid water is a common phenomenon beyond this ARM
597 site in EAMv1 modeled mixed-phase clouds (figures not shown). Results based on the global
598 evaluation of EAMv1 simulated mixed-phase clouds will be reported in a separate paper. As
599 indicated in earlier studies, cloud feedback and climate sensitivity can be strongly influenced by
600 the phase partitioning in mixed-phase clouds (Tan & Storelvmo, 2019; Tan et al., 2016). The
601 biased phase partitioning of condensate in low-level mixed-phase clouds identified in this study
602 may introduce biases to the cloud feedback and climate sensitivity estimated by E3SM (Golaz et
603 al., 2019), which is also of interest in the future study.

604

Acknowledgements: This research was primarily supported by the DOE Atmospheric System Research (ASR) Program (grants DE-SC0020510) and the Energy Exascale Earth System Model (E3SM) project and partially funded by the DOE Regional and Global Model Analysis program area (RGMA) and ASR's Cloud-Associated Parameterizations Testbed (CAPT) project and the Climate Model Development and Validation (CMDV) activity, funded by the U.S. Department of Energy, Office of Science, Office of Biological and Environmental Research. The model data used in this study can be downloaded at http://portal.nersc.gov/project/m2136/E3SMv1/Zhang-SLF. Work at LLNL was performed under the auspices of the U.S. DOE by Lawrence Livermore National Laboratory under contract No. DE-AC52-07NA27344. The Pacific Northwest National Laboratory (PNNL) is operated for the DOE by Battelle Memorial Institute under contract DE-AC06-76RLO 1830. We also appreciate Hunter Brown at University of Wyoming for his help with the grammar. This research used high-performance computing resources from the National Energy Research Scientific Computing Center, a DOE Office of Science User Facility supported by the Office of Science of the U.S. Department of Energy under Contract No. DE-AC02-05CH11231. The ARM M-PACE observational dataset is available from DOE ARM website (https://www.archive.arm.gov/discovery/).

Table and Figures

Table 1. *Summary of Physical Parameterizations in EAMv1 Simulations*

Experiment	Configurations	Note
CTL	Parameter "berg_eff_factor" change to 1.0	Same as default EAMv1, but use the value 1.0 for the parameter that controls the WBF rate.
MEYERS	Same as CTL, but replace the CNT ice nucleation scheme (Wang et al., 2014) with Meyers et al. (1992)	Examine the effect of heterogeneous ice nucleation. Note that the Meyers scheme generally produces higher INP number concentrations than CNT.
UW	Same as CTL, but replace CLUBB with the CAM5 UW shallow convection, PBL turbulence, and cloud macrophysical schemes (Park and Bretherton, 2009; Bretherton and Park 2009; Park et al. 2014)	Examine the effect of CLUBB.
UW_MG1	Same as UW, except using the MG1 microphysics	Examine the effect of updated cloud microphysics.

625 Table 2. *Summary of M-PACE Observations Used in This Study*

Observation	Quantity	Source and reference
ACRED	LWC/LWP and IWC/IWP	ARM cloud retrieval ensemble dataset (ACRED; Zhao et al., 2012)
ARSCL	Cloud fraction	Active Remotely Sensed Clouds Locations (ARSCL) algorithm (Clothiaux et al., 2000)
UND Citation	LWC and IWC	University of North Dakota (UND) Citation aircraft (McFarquhar et al., 2007)

626

627 Figure 1. Time-pressure cross sections of cloud fraction at the NSA Utqiaġvik site during the M-
628 PACE field campaign. (a) Observed frequency of occurrence of clouds from the Active
629 Remotely Sensed Clouds Locations (ARSCL) algorithm. (b) Simulated cloud fraction from CTL.
630 (c)-(e) are the differences in simulated cloud fraction between (c) CTL and MEYERS, (d) CTL
631 and UW, and (e) UW and UW_MG1. Unit: %. Note that CTL utilizes CLUBB, MG2, and CNT
632 parameterizations, while three sensitivity experiments have changes of Meyers et al. (1992) ice
633 nucleation (MEYERS), UW shallow convection, PBL turbulence, and cloud macrophysics
634 parameterizations (UW), and both UW schemes and MG1 cloud microphysics (UW_MG1),
635 respectively.

636

637 Figure 2. Time-pressure cross sections of simulated total cloud liquid water mass mixing ratio
638 (including rain water mass; upper panel), total cloud ice water mass mixing ratio (including snow
639 water mass; middle panel), and supercooled liquid fraction (lower panel) during the M-PACE
640 field campaign from CTL, MEYERS, UW, and UW_MG1 (from left to right). (a)-(d) are for

641 cloud liquid water, (e)-(h) are for cloud ice water mass, and (i)-(l) are for supercooled liquid
642 fraction. Contours represent the ambient temperature in the unit of °C.

643

644 Figure 3. Time-pressure cross sections of simulated grid mean cloud ice number concentrations
645 for the M-PACE. (a) CTL, (b) MEYERS, (c) UW, and (d) UW_MG1. Contours represent the
646 ambient temperature in the unit of °C.

647

648 Figure 4. Time series of liquid water path (including rain; upper panel) and ice water path
649 (including snow; lower panel) from the EAMv1 and the ARM ACRED dataset between 9-15
650 October. CTL is presented by red solid line, MEYERS green solid line, UW blue solid line, and
651 UW_MG1 brown solid line. For the ACRED dataset, grey lines represent the one standard
652 deviation for each data point.

653

654 Figure 5. Distribution of supercooled liquid fraction as a function of normalized height in clouds.
655 (a) The in-situ measurements obtained from the University of North Dakota Citation aircraft
656 (McFarquhar et al., 2007) on 9 October (black dots), 10 October (red dots), and 12 October (blue
657 dots) during the M-PACE field campaign. (b)-(e) Results of model simulations from CTL,
658 MEYERS, UW, and UW_MG1, respectively. Model results are sampled on 9, 10, 12 October
659 which correspond to the same time period as the measurements.

660

661 Figure 6. Budgets of vertically integrated cloud physical process tendencies of (a) cloud liquid,
662 (b) rain, (c) cloud ice, and (d) snow hydrometeors from the short-term hindcast day-2 results of
663 CTL (red bars) and three sensitivity experiments, which are MEYERS (green bars), UW (blue
664 bars), and UW_MG1 (brown bars). The vertically integrated process rates are averaged over 3-
665 day period between 9 and 11 October 2004 during the M-PACE field campaign.

666

667

References

Barrett, A. I., Hogan, R. J., & Forbes R. M. (2017). Why are mixed-phase altocumulus clouds poorly predicted by large-scale models? Part 1. Physical processes. *Journal of Geophysical Research: Atmospheres*, 122, 9903-9926. https://doi.org/10.1002/2016JD026321

Bennartz, R., Shupe, M. D., Turner, D. D., Walden, V. P., Steffen, K., Cox, C. J., et al. (2013). July 2012 Greenland melt extent enhanced by low-level liquid clouds. *Nature*, 496, 83-86. https://doi.org/10.1038/nature12002

Bogenschutz, P. A., Gettelman, A., Morrison, H., Larson, V. E., Craig, C., & Schanen, D. P. (2013). Higher-order turbulence closure and its impact on climate simulations in the Community Atmosphere Model. *Journal of Climate*, 26(23), 9655–9676. https://doi.org/10.1175/JCLI-D-13-00075.1

Bogenschutz, P. A., Gettelman, A., Morrison, H., Larson, V. E., Schanen, D. P., Meyer, N. R., et al. (2012). Unified parameterization of the planetary boundary layer and shallow convection with a higher-order turbulence closure in the Community Atmosphere Model: single-column experiments. *Geoscientific Model Development*, 5, 1407-1423. https://doi.org/10.5194/gmd-5-1407-2012, 2012

688 Bretherton, C. S. & Park, S. (2009). A New Moist Turbulence Parameterization in the
689 Community Atmosphere Model. *Journal of Climate*, 22, 3422-3448.
690 https://doi.org/10.1175/2008JCLI2556.1

691

692 Clothiaux, E. E., Ackerman, T. P., Mace, G. G., Moran, K. P., Marchand, R. T., Miller, M. A., &
693 Martner, B. E. (2000). Objective determination of cloud heights and radar reflectivities using a
694 combination of active remote sensors at the ARM CART sites. *Journal of Applied Meteorology*
695 *and Climatology*, 39, 645-665. https://doi.org/10.1175/1520-
696 0450(2000)039%3C0645:ODOCHA%3E2.0.CO;2

697

698 de Boer, G., Eloranta, E. W., & Shupe, M. D. (2009). Arctic Mixed-Phase Stratiform Cloud
699 Properties from Multiple Years of Surface-Based Measurements at Two High-Latitude
700 Locations. *Journal of the Atmospheric Science*, 66, 2874-2887.
701 https://doi.org/10.1175/2009JAS3029.1

702

703 Dee, D. P., Uppala, S. M., Simmons, A. J., Berrisford, P., Poli, P., Kobayashi, S., et al. (2011).
704 The ERA-Interim reanalysis: configuration and performance of the data assimilation system.
705 *Quarterly Journal of the Royal Meteorological Society*, 137, 553-597.
706 https://doi.org/10.1002/qj.828

707

DeMott, P. J., Prenni, A. J., Liu, X., Kreidenweis, S. M., Petters, M. D., Twohy, C. H., et al. (2010). Predicting global atmospheric ice nuclei distributions and their impacts on climate. *Proceedings of the National Academy of Sciences*, 107(25), 11217-11222. https://doi.org/10.1073/pnas.0910818107

DeMott, P. J., Prenni, A. J., McMeeking, G. R., Sullivan, R. C., Petters, M. D., Tobo, Y., et al. (2015). Integrating laboratory and field data to quantify the immersion freezing ice nucleation activity of mineral dust particles. *Atmospheric Chemistry and Physics*, 15(1), 393-409. https://doi.org/10.5194/acp-15-393-2015

Dong, X., & Mace, G. G. (2003). Profiles of low-level stratus cloud microphysics deduced from ground-based measurements. *Journal of Atmospheric and Oceanic Technology*, 20, 42-53. https://doi.org/10.1175/1520-0426(2003)020<0042:POLLSC>2.0.CO;2

Field, P. R., Lawson, R. P., Brown, P. R., Lloyd, G., Westbrook, C., Moisseev, D., et al. (2017). Secondary ice production: Current state of the science and recommendations for the future. *Meteorological Monographs*, 58, 7.1-7.20. https://doi.org/10.1175/AMSMONOGRAPHS-D-16-0014.1

727 Frisch, A. S., Fairall, C. W. & Snider, J. B. (1995). Measurement of stratus cloud and drizzle
728 parameters in ASTEX with Ka-band Doppler radar and a microwave radiometer. *Journal of the*
729 *Atmospheric Science*. 52, 2788-2799. https://doi.org/10.1175/1520-
730 0469(1995)052<2788:MOSCAD>2.0.CO;2

731

732 Gettelman, A., Liu, X., Ghan, S. J., Morrison, H., Park, S., Conley, A. J., et al. (2010). Global
733 simulations of ice nucleation and ice supersaturation with an improved cloud scheme in the
734 Community Atmosphere Model. *Journal of Geophysical Research: Atmospheres*, 115, D18216.
735 https://doi.org/10.1029/2009JD013797

736

737 Gettelman, A., & Morrison, H. (2015). Advanced two-moment bulk microphysics for global
738 models. Part I: Off-line tests and comparison with other schemes. *Journal of Climate*, 28(3),
739 1268-1287. https://doi.org/10.1175/JCLI-D-14-00102.1

740

741 Gettelman, A., Morrison, H., Santos, S., Bogenschutz, P. & Caldwell, P. M. (2015). Advanced
742 Two-Moment Bulk Microphysics for Global Models. Part II: Global Model Solutions and
743 Aerosol–Cloud Interactions. *Journal of Climate*, 28, 1288-1307. https://doi.org/10.1175/JCLI-D-
744 14-00103.1

745

746 Golaz, J.-C., Caldwell, P. M., Van Roekel, L. P., Petersen, M. R., Tang, Q., Wolfe, J. D., et al.
747 (2019). The DOE E3SM coupled model version 1: Overview and evaluation at standard
748 resolution. *Journal of Advances in Modeling Earth*
749 *Systems*, 11. https://doi.org/10.1029/2018MS001603

750

751 Golaz, J.-C., Larson, V. E., & Cotton, W. R. (2002). A PDF-based model for boundary layer
752 clouds. Part I: Method and model description. *Journal of the Atmospheric Sciences*, 59(24),
753 3540–3551. https://doi.org/10.1175/1520-0469(2002)059<3540:APBMFB>2.0.CO;2

754

755 Hofer, S., Tedstone, A. J., Fettweis, X. & Bamber, J. L. (2019). Cloud microphysics and
756 circulation anomalies control differences in future Greenland melt. *Nature Climate Change*, 9,
757 523-528. https://doi.org/10.1038/s41558-019-0507-8

758

759 Hoose, C., Kristjánsson, J. E., Chen, J. P., & Hazra, A. (2010). A classical-theory-based
760 parameterization of heterogeneous ice nucleation by mineral dust, soot, and biological particles
761 in a global climate model. *Journal of the Atmospheric Sciences*, 67, 2483-2503.
762 https://doi.org/10.1175/2010JAS3425.1

763

764 Hsu, J., & Prather, M. J. (2009). Stratospheric variability and tropospheric ozone. *Journal of*
765 *Geophysical Research*, 114, D06102. https://doi.org/10.1029/2008JD010942

Ivanova, D. C., Mitchell, D. L., Arnott, W. P., & Poellot, M. (2001). A GCM parameterization for bimodal size spectra and ice mass removal rates in mid-latitude cirrus clouds. *Atmospheric Research*, 59-60, 89-113. https://doi.org/10.1016/S0169-8095(01)00111-9.

Kay, J. E., Bourdages, L., Miller, N. B., Morrison, A., Yettella, V., Chepfer, H. & Eaton, B. (2016). Evaluating and improving cloud phase in the Community Atmosphere Model version 5 using spaceborne lidar observations, *Journal of Geophysical Research: Atmospheres*, 121, 4162-4176. https://doi.org/10.1002/2015JD024699

Klein, S. A., McCoy, R. B., Morrison, H., Ackerman, A. S., Avramov, A., Boer, G. d., et al. (2009). Intercomparison of model simulations of mixed-phase clouds observed during the ARM Mixed-Phase Arctic Cloud Experiment. I: single-layer cloud. *Quarterly Journal of the Royal Meteorological Society*, 135: 979-1002. https://doi.org/10.1002/qj.416

Komurcu, M., Storelvmo, T., Tan, I., Lohmann, U., Yun, Y., Penner, J. E., et al. (2014). Inter-comparison of the cloud water phase among global climate models, *Journal of Geophysical Research: Atmospheres*, 119, 3372-3400. https://doi.org/10.1002/2013JD021119

Larson, V. E. (2017). CLUBB-SILHS: A parameterization of subgrid variability in the atmosphere. *ArXiv:1711.03675 [Physics]*. Retrieved from http://arxiv.org/abs/1711.03675

Larson, V. E., & Golaz, J.-C. (2005). Using probability density functions to derive consistent closure relationships among higher-order moments. *Monthly Weather Review*, 133(4), 1023-1042. https://doi.org/10.1175/MWR2902.1

Larson, V. E., Golaz, J. & Cotton, W. R. (2002). Small-Scale and Mesoscale Variability in Cloudy Boundary Layers: Joint Probability Density Functions. *Journal of the Atmospheric Sciences*, 59, 3519-3539. https://doi.org/10.1175/1520-0469(2002)059<3519:SSAMVI>2.0.CO;2

Lawson, P. R., & Gettelman, A. (2014). Impact of Antarctic clouds on climate. *Proceedings of the National Academy of Sciences*, 111(51), 18156-18161. https://doi.org/10.1073/pnas.1418197111

Liao, L., & Sassen, K. (1994), Investigation of relationships between Ka-band radar reflectivity and ice and liquid water contents. *Atmospheric Research*, 34, 231-248. https://doi.org/10.1016/0169-8095(94)90094-9

Liu, C.-L., & Illingworth, A. J. (2000). Towards more accurate retrievals of ice water content from radar measurement of clouds, J *Journal of Applied Meteorology and Climatology*, 39, 1130-1146. https://doi.org/10.1175/1520-0450(2000)039<1130:TMAROI>2.0.CO;2

Liu, X., Ma, P.-L., Wang, H., Tilmes, S., Singh, B., Easter, R. C., et al. (2016). Description and evaluation of a new four-mode version of the Modal Aerosol Module (MAM4) within version 5.3 of the Community Atmosphere Model. *Geoscientific Model Development*, 9(2), 505-522. https://doi.org/10.5194/gmd-9-505-2016

Liu, X., Xie, S., Boyle, J., Klein, S. A., Shi, X., Wang, Z., et al. (2011). Testing cloud microphysics parameterizations in NCAR CAM5 with ISDAC and M-PACE observations. *Journal of Geophysical Research: Atmospheres*, 116, D00T11. https://doi.org/10.1029/2011JD015889

Lohmann, U. & Neubauer, D. (2018). The importance of mixed-phase and ice clouds for climate sensitivity in the global aerosol–climate model ECHAM6-HAM2. *Atmospheric Chemistry and Physics*, 18, 8807-8828. https://doi.org/10.5194/acp-18-8807-2018

Ma, H.-Y., Chuang, C. C., Klein, S. A., Lo, M.-H., Zhang, Y., Xie, S., et al. (2015). An improved hindcast approach for evaluation and diagnosis of physical processes in global climate models. *Journal of Advances in Modeling Earth Systems*, 7, 1810-1827. https://doi.org/10.1002/2015MS000490

Ma, H.-Y., Xie, S., Boyle, J. S., Klein, S. A., & Zhang, Y. (2013). Metrics and diagnostics for precipitation-related processes in climate model short-range hindcasts. *Journal of Climate*, 26, 1516–1534. https://doi.org/10.1175/JCLI-D-12-00235.1

Ma, H.-Y., Xie, S., Klein, S. A., Williams, K. D., Boyle, J. S., Bony, S., et al. (2014). On the correspondence between mean forecast errors and climate errors in CMIP5 models. *Journal of Climate*, 27(4), 1781-1798. https://doi.org/10.1175/JCLI-D-13-00474.1

McCoy, D. T., Hartmann, D. L., Zelinka, M. D., Ceppi, P., & Grosvenor, D. P. (2015). Mixed-phase cloud physics and Southern Ocean cloud feedback in climate models. *Journal of Geophysical Research: Atmospheres*, 120, 9539-9554. https://doi.org/10.1002/2015JD023603

McCoy, D. T., Tan, I., Hartmann, D. L., Zelinka, M. D., & Storelvmo, T. (2016). On the relationships among cloud cover, mixed-phase partitioning, and planetary albedo in

GCMs. *Journal of Advances in Modeling Earth Systems*, 8, 650-668. https://doi.org/10.1002/2015MS000589

McFarquhar, G. M., Zhang, G., Poellot, M. R., Kok, G. L., McCoy, R., Tooman, T., et al. (2007). Ice properties of single-layer stratocumulus during the Mixed-Phase Arctic Cloud Experiment: 1. Observations. *Journal of Geophysical Research: Atmospheres*, 112, D24201. https://doi.org/10.1029/2007JD008633

McLinden, C. A., Olsen, S. C., Hannegan, B. J., Wild, O., and Prather, M. J. (2000). Stratosphere ozone in 3-D models: A simple chemistry and the cross-tropopause flux, *Journal of Geophysical Research: Atmospheres*, 105(D11), 14,653–14,665. https://doi.org/10.1029/2000JD900124

Meyers, M. P., DeMott, P. J., & Cotton, W. R. (1992). New primary ice-nucleation parameterizations in an explicit cloud model. *Journal of Applied Meteorology and Climatology*, 31, 708-721. https://doi.org/10.1175/1520-0450(1992)031<0708:NPINPI>2.0.CO;2

Morrison, H., & Gettelman, A. (2008). A new two-moment bulk stratiform cloud microphysics scheme in the Community Atmosphere Model, version 3 (CAM3). Part I: Description and numerical tests. *Journal of Climate*, 21(15), 3642-3659. https://doi.org/10.1175/2008JCLI2105.1

Morrison, H., McCoy, R. B., Klein, S. A., Xie, S., Luo, Y., Avramov, A., et al. (2009). Intercomparison of model simulations of mixed-phase clouds observed during the ARM Mixed-Phase Arctic Cloud Experiment. II: Multilayer cloud. *Quarterly Journal of the Royal Meteorological Society*, 135: 1003-1019. https://doi.org/10.1002/qj.415

Nicolas, J. P., Vogelmann, A. M., Scott, R. C., Wilson, A. B., Cadeddu, M. P., Bromwich, D. H., et al. (2017). January 2016 extensive summer melt in West Antarctica favoured by strong El Niño. *Nature Communications*, 8, 15799. https://doi.org/10.1038/ncomms15799

Niemand, M., Möhler, O., Vogel, B., Vogel, H., Hoose, C., Connolly, P., et al. (2012). A Particle-Surface-Area-Based Parameterization of Immersion Freezing on Desert Dust Particles. *Journal of the Atmospheric Sciences*, 69, 3077-3092. https://doi.org/10.1175/JAS-D-11-0249.1

Park, S., & Bretherton, C. S. (2009). The University of Washington shallow convection and moist turbulence schemes and their impact on climate simulations with the Community Atmosphere Model. *Journal of Climate*, 22, 3449-3469. https://doi.org/10.1175/2008JCLI2557.1

881 Park, S., Bretherton, C. S., & Rasch, P. J. (2014). Integrating Cloud Processes in the Community
882 Atmosphere Model, Version 5. *Journal of Climate*, 27, 6821-6856. https://doi.org/10.1175/JCLI-
883 D-14-00087.1

884

885 Phillips, T. J., Potter, G. L., Williamson, D. L., Cederwall, R. T., Boyle, J. S., Fiorino, M., et al.
886 (2004). Evaluating Parameterizations in General Circulation Models: Climate Simulation Meets
887 Weather Prediction. *Bulletin of the American Meteorological Society*, 85, 1903-
888 1916. https://doi.org/10.1175/BAMS-85-12-1903

889

890 Prenni, A. J., Harrington, J. Y., Tjernström, M., DeMott, P. J., Avramov, A., Long, C. N., et al.
891 (2007). Can ice-nucleating aerosols affect arctic seasonal climate? *Bulletin of the American*
892 *Meteorological Society*, 88(4), 541-550. https://doi.org/10.1175/BAMS-88-4-541

893

894 Qian, Y., Wan, H., Yang, B., Golaz, J.-C., Harrop, B., Hou, Z., et al. (2018). Parametric
895 sensitivity and uncertainty quantification in the version 1 of E3SM atmosphere model based on
896 short perturbed parameter ensemble simulations. *Journal of Geophysical Research:*
897 *Atmospheres*, 123, 13,046–13,073. https://doi.org/10.1029/2018JD028927

898

Rasch, P. J., Xie, S., Ma, P.-L., Lin, W., Wang, H., Tang, Q., et al. (2019). An Overview of the Atmospheric Component of the Energy Exascale Earth System Model. *Journal of Advances in Modeling Earth Systems*, 11, 2377– 2411. https://doi.org/10.1029/2019MS001629

Shi, Y., & Liu, X. (2019). Dust radiative effects on climate by glaciating mixed-phase clouds. *Geophysical Research Letters*, 46. https://doi.org/10.1029/2019GL082504

Shupe, M. D., Matrosov, S. Y., & Uttal, T. (2006). Arctic Mixed-Phase Cloud Properties Derived from Surface-Based Sensors at SHEBA. *Journal of the Atmospheric Sciences*, 63, 697-711. https://doi.org/10.1175/JAS3659.1

Shupe, M. D., Uttal, T., & Matrosov, S. Y. (2005), Arctic cloud microphysics retrievals from surface-based remote sensors at SHEBA. *Journal of Applied Meteorology and Climatology*, 44, 1544-1562. https://doi.org/10.1175/JAM2297.1

Shupe, M. D., Walden, V. P., Eloranta, E., Uttal, T., Campbell, J. R., Starkweather, S. M. et al. (2011). Clouds at Arctic Atmospheric Observatories. Part I: Occurrence and Macrophysical Properties. *Journal of Applied Meteorology and Climatology*, 50, 626-644. https://doi.org/10.1175/2010JAMC2467.1

Storelvmo, T., Kristjánsson, J. E., Lohmann, U., Iversen, T., Kirkevåg, A., & Seland, Ø. (2008). Modeling of the Wegener-Bergeron-Findeisen process—implications for aerosol indirect effects. *Environmental Research Letters*, 3, 045001. https://doi.org/10.1088/1748-9326/3/4/045001

Tan, I., & Storelvmo, T. (2016). Sensitivity study on the influence of cloud microphysical parameters on mixed-phase cloud thermodynamic phase partitioning in CAM5. *Journal of the Atmospheric Sciences,* 73, 709-728. https://doi.org/10.1175/JAS-D-15-0152.1

Tan, I., & Storelvmo, T. (2019). Evidence of strong contributions from mixed-phase clouds to Arctic climate change. *Geophysical Research Letters*, 46, 2894-2902. https://doi.org/10.1029/2018GL081871

Tan, I., Storelvmo, T., & Zelinka, M. D. (2016). Observational constraints on mixed-phase clouds imply higher climate sensitivity. *Science*, 352, 224-227. https://doi.org/10.1126/science.aad5300

Turner, D. (2005). Arctic mixed-phase cloud properties from AERI-lidar observations: Algorithm and results from SHEBA. *Journal of Applied Meteorology and Climatology*, 44, 427-444. https://doi.org/10.1175/JAM2208.1

939

940 Verlinde, J., Harrington, J. Y., McFarquhar, G. M., Yannuzzi, V. T., Avramov, A., Greenberg,
941 S., et al. (2007). The Mixed-Phase Arctic Cloud Experiment. *Bulletin of the American*
942 *Meteorological Society*, 88, 205-222. https://doi.org/10.1175/BAMS-88-2-205

943

944 Wang, H., Easter, R. C., Rasch, P. J., Wang, M., Liu, X., Ghan, S. J., et al. (2013). Sensitivity of
945 remote aerosol distributions to representation of cloud-aerosol interactions in a global climate
946 model. *Geoscientific Model Development*, 6(3), 765–782. https://doi.org/10.5194/gmd-6-
947 765-2013

948

949 Wang, Y., Liu, X., Hoose, C., & Wang, B. (2014). Different contact angle distributions for
950 heterogeneous ice nucleation in the Community Atmospheric Model version 5. *Atmospheric*
951 *Chemistry and Physics*, 14, 10411-10430. https://doi.org/10.5194/acp-14-10411-2014

952

953 Wang, Y., Zhang, D., Liu, X., & Wang, Z. (2018). Distinct contributions of ice nucleation, large-
954 scale environment, and shallow cumulus detrainment to cloud phase partitioning with NCAR
955 CAM5. *Journal of Geophysical Research: Atmospheres*, 123, 1132-1154.
956 https://doi.org/10.1002/2017JD027213

957

Wang, Z., & K. Sassen (2002). Cirrus cloud microphysical property retrieval using lidar and radar measurements: I. Algorithm description and comparison with in situ data. *Journal of Applied Meteorology and Climatology*, 41, 218-229. https://doi.org/10.1175/1520-0450(2002)041<0218:CCMPRU>2.0.CO;2

Wang, Z., Sassen, K., Whiteman, D. N., & Demoz, B. B. (2004). Studying altocumulus with ice virga using ground-based active and passive remote sensors. *Journal of Applied Meteorology and Climatology*, 43, 449-460. https://doi.org/10.1175/1520-0450(2004)043<0449:SAWIVU>2.0.CO;2

Williams, K. D. & Brooks, M. E. (2008). Initial Tendencies of Cloud Regimes in the Met Office Unified Model. *Journal of Climate*, 21, 833–840. https://doi.org/10.1175/2007JCLI1900.1

Xie, S., Boyle, J., Klein, S. A., Liu, X., & Ghan, S. (2008). Simulations of Arctic mixed-phase clouds in forecasts with CAM3 and AM2 for M-PACE. *Journal of Geophysical Research: Atmospheres*, 113, D04211. https://doi.org/10.1029/2007JD009225

Xie, S., Klein, S. A., Yio, J. J., Beljaars, A. C. M., Long, C. N., & Zhang, M. (2006). An assessment of ECMWF analyses and model forecasts over the North Slope of Alaska using

977 observations from the ARM Mixed-Phase Arctic Cloud Experiment. *Journal of Geophysical*
978 *Research: Atmospheres*, 111, D05107. https://doi.org/10.1029/2005JD006509

979

980 Xie, S., Lin, W., Rasch, P. J., Ma, P.-L., Neale, R., Larson, V. E., et al. (2018). Understanding
981 cloud and convective characteristics in version 1 of the E3SM atmosphere model. *Journal of*
982 *Advances in Modeling Earth Systems*, 10, 2618-2644. https://doi.org/10.1029/2018MS001350

983

984 Xie, S., Liu, X., Zhao, C., & Zhang, Y. (2013). Sensitivity of CAM5-Simulated Arctic Clouds
985 and Radiation to Ice Nucleation Parameterization. *Journal of Climate*, 26, 5981-5999.
986 https://doi.org/10.1175/JCLI-D-12-00517.1

987

988 Xie, S., Ma, H.-Y., Boyle, J. S., Klein, S. A., & Zhang, Y. (2012). On the correspondence
989 between short- and long-time-scale systematic errors in CAM4/CAM5 for the year of tropical
990 convection. *Journal of Climate*, 25(22), 7937-7955. https://doi.org/10.1175/JCLI-D-12-00134.1

991

992 Zhang, D., Vogelmann, A., Kollias, P., Luke, E., Yang, F., Lubin, D., & Wang, Z. (2019).
993 Comparison of Antarctic and Arctic single-layer stratiform mixed-phase cloud properties using
994 ground-based remote sensing measurements. *Journal of Geophysical Research: Atmospheres*,
995 124(17-18), 10186-10204. https://doi.org/10.1029/2019JD030673

Zhang, K., Rasch, P. J., Taylor, M. A., Wan, H., Leung, R., Ma, P.-L., et al. (2018). Impact of numerical choices on water conservation in the E3SM Atmosphere Model version 1 (EAMv1). *Geoscientific Model Development*, 11, 1971-1988. https://doi.org/10.5194/gmd-11-1971-2018

Zhang, K., Wan, H., Liu, X., Ghan, S. J., Kooperman, G. J., Ma, P.-L., et al. (2014). Technical Note: On the use of nudging for aerosol–climate model intercomparison studies. *Atmospheric Chemistry and Physics*, 14, 8631–8645. https://doi.org/10.5194/acp-14-8631-2014

Zhang, G. J., & McFarlane, N. A. (1995). Sensitivity of climate simulations to the parameterization of cumulus convection in the Canadian Climate Centre general circulation model. *Atmosphere-Ocean*, 33(3), 407-446. https://doi.org/10.1080/07055900.1995.9649539

Zhang, M., Liu, X., Diao, M., D'Alessandro, J. J., Wang, Y., Wu, C., et al. (2019). Impacts of representing heterogeneous distribution of cloud liquid and Ice on phase partitioning of Arctic mixed-phase clouds. *Journal of Geophysical Research: Atmospheres*, 124. https://doi.org/10.1029/2019JD030502

Zhang, Y., Xie, S., Covey, C., Lucas, D. D., Gleckler, P., Klein, S. A., et al. (2012), Regional assessment of the parameter-dependent performance of CAM4 in simulating tropical clouds. *Geophysical Research Letters*, 39, L14708. https://doi.org/10.1029/2012GL052184

Zhang, Y., Xie, S., Lin, W., Klein, S. A., Zelinka, M., Ma, P.-L., et al. (2019). Evaluation of clouds in version 1 of the E3SM atmosphere model with satellite simulators. *Journal of Advances in Modeling Earth Systems*, 11, 1253-1268. https://doi.org/10.1029/2018MS001562

Zhao, C., Xie, S., Klein, S. A., Protat, A., Shupe, M. D., McFarlane, S. A. et al. (2012). Toward understanding of differences in current cloud retrievals of ARM ground-based measurements, *Journal of Geophysical Research: Atmospheres*, 117, D10206. https://doi.org/10.1029/2011JD016792

Zheng, X., Klein, S. A., Ma, H.-Y., Bogenschutz, P., Gettelman, A., & Larson, V. E. (2016). Assessment of marine boundary layer cloud simulations in the CAM with CLUBB and updated microphysics scheme based on ARM observations from the Azores. *Journal of Geophysical Research: Atmospheres*, 121, 8472-8492, https://doi.org/10.1002/2016JD025274

1 **Table and Figures**

2 Table 1. *Summary of Physical Parameterizations in EAMv1 Simulations*

Experiment	Configurations	Note
CTL	Parameter "berg_eff_factor" change to 1.0	Same as default EAMv1, but use the value 1.0 for the parameter that controls the WBF rate.
MEYERS	Same as CTL, but replace the CNT ice nucleation scheme (Wang et al., 2014) with Meyers et al. (1992)	Examine the effect of heterogeneous ice nucleation. Note that the Meyers scheme generally produces higher INP number concentrations than CNT.
UW	Same as CTL, but replace CLUBB with the CAM5 UW shallow convection, PBL turbulence, and cloud macrophysical schemes (Park and Bretherton, 2009; Bretherton and Park 2009; Park et al. 2014)	Examine the effect of CLUBB.
UW_MG1	Same as UW, except using the MG1 microphysics	Examine the effect of updated cloud microphysics.

3

4

Table 2. *Summary of M-PACE Observations Used in This Study*

Observation	Quantity	Source and reference
ACRED	LWP and IWP	ARM cloud retrieval ensemble dataset (ACRED; Zhao et al., 2012)
ARSCL	Cloud fraction	Active Remotely Sensed Clouds Locations (ARSCL) algorithm (Clothiaux et al., 2000)
UND Citation	LWC and IWC	University of North Dakota (UND) Citation aircraft (McFarquhar et al., 2007)

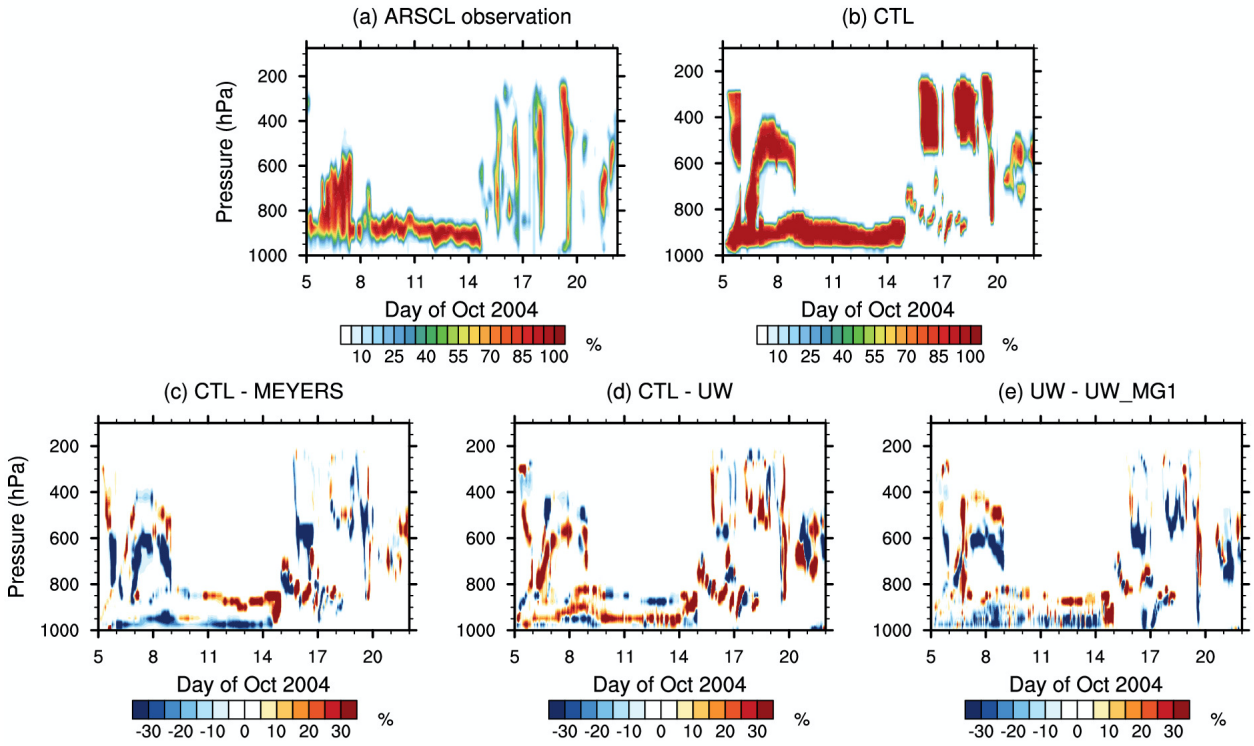

Figure 1. Time-pressure cross sections of cloud fraction at the NSA Barrow site during the M-PACE field campaign. (a) Observed frequency of occurrence of clouds from the Active Remotely Sensed Clouds Locations (ARSCL) algorithm. (b) Simulated cloud fraction from CTL. (c)-(e) are the differences in simulated cloud fraction between (c) CTL and MEYERS, (d) CTL and UW, and (e) UW and UW_MG1. Unit: %. Note that CTL utilizes CLUBB, MG2, and CNT parameterizations, while three sensitivity experiments have changes of Meyers et al. (1992) ice nucleation (MEYERS), UW shallow convection, PBL turbulence, and cloud macrophysics parameterizations (UW), and both UW schemes and MG1 cloud microphysics (UW_MG1), respectively.

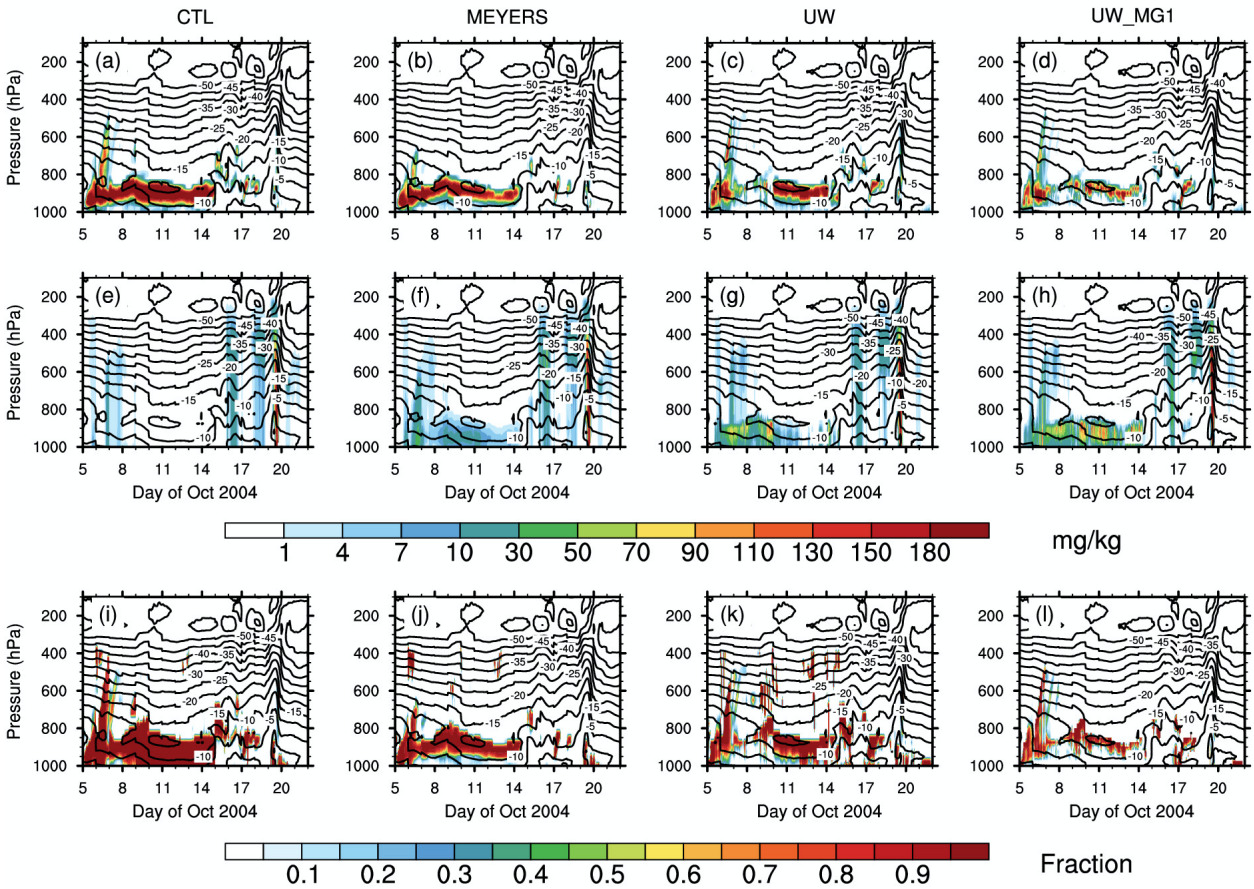

Figure 2. Time-pressure cross sections of simulated total cloud liquid water mass mixing ratio (including rain water mass; upper panel), total cloud ice water mass mixing ratio (including snow water mass; middle panel), and supercooled liquid fraction (lower panel) during the M-PACE field campaign from CTL, MEYERS, UW, and UW_MG1 (from left to right). (a)-(d) are for cloud liquid water, (e)-(h) are for cloud ice water mass, and (i)-(l) are for supercooled liquid fraction. Contours represent the ambient temperature in the unit of °C.

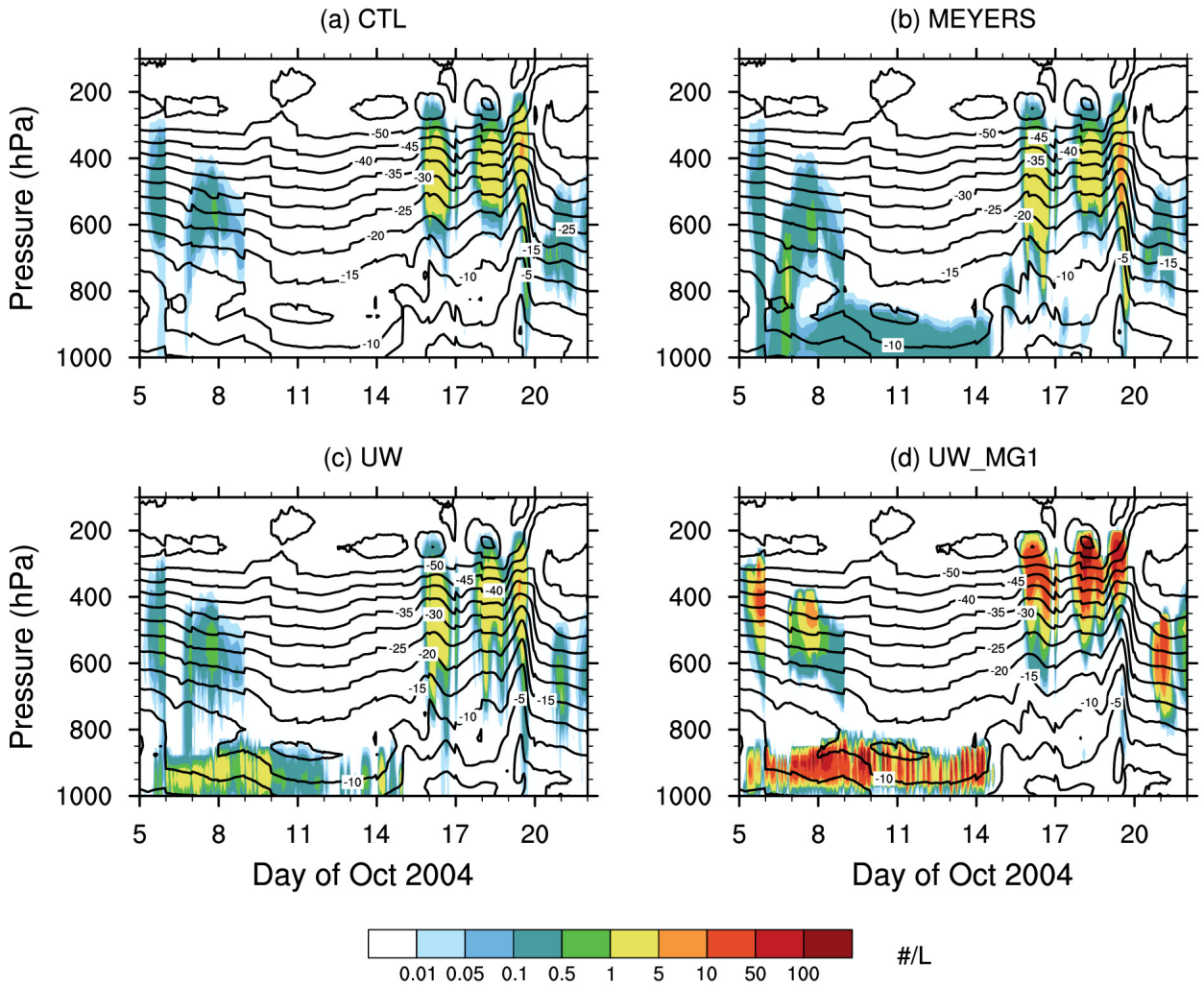

27

28 Figure 3. Time-pressure cross sections of simulated grid mean cloud ice number concentrations

29 for the M-PACE. (a) CTL, (b) MEYERS, (c) UW, and (d) UW_MG1. Contours represent the

30 ambient temperature in the unit of °C.

31

32

33

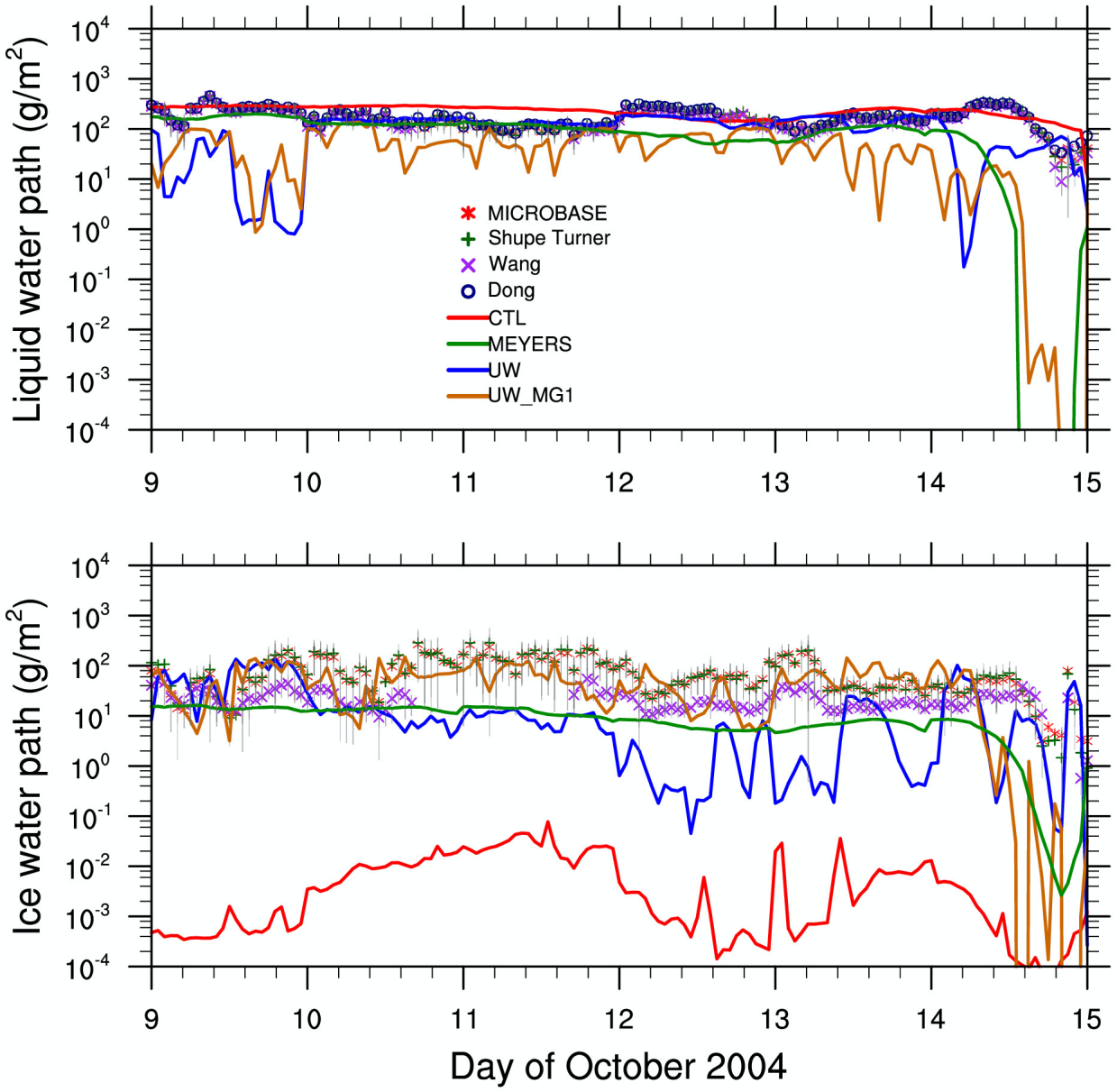

Figure 4. Time series of liquid water path (including rain; upper panel) and ice water path (including snow; lower panel) from the EAMv1 and the ARM ACRED dataset between 9-15 October. CTL is presented by red solid line, MEYERS green solid line, UW blue solid line, and

UW_MG1 brown solid. For the ACRED dataset, red star is the MICROBASE observation. Green plus is the retrieval from Shupe (2007). Purple cross represents the retrieval products from Wang et al., (2004). Dark blue circle is from Dong and Mace (2003), and orange triangle is from Deng and Mace (2006). Grey lines represent the one standard deviation for each data point.

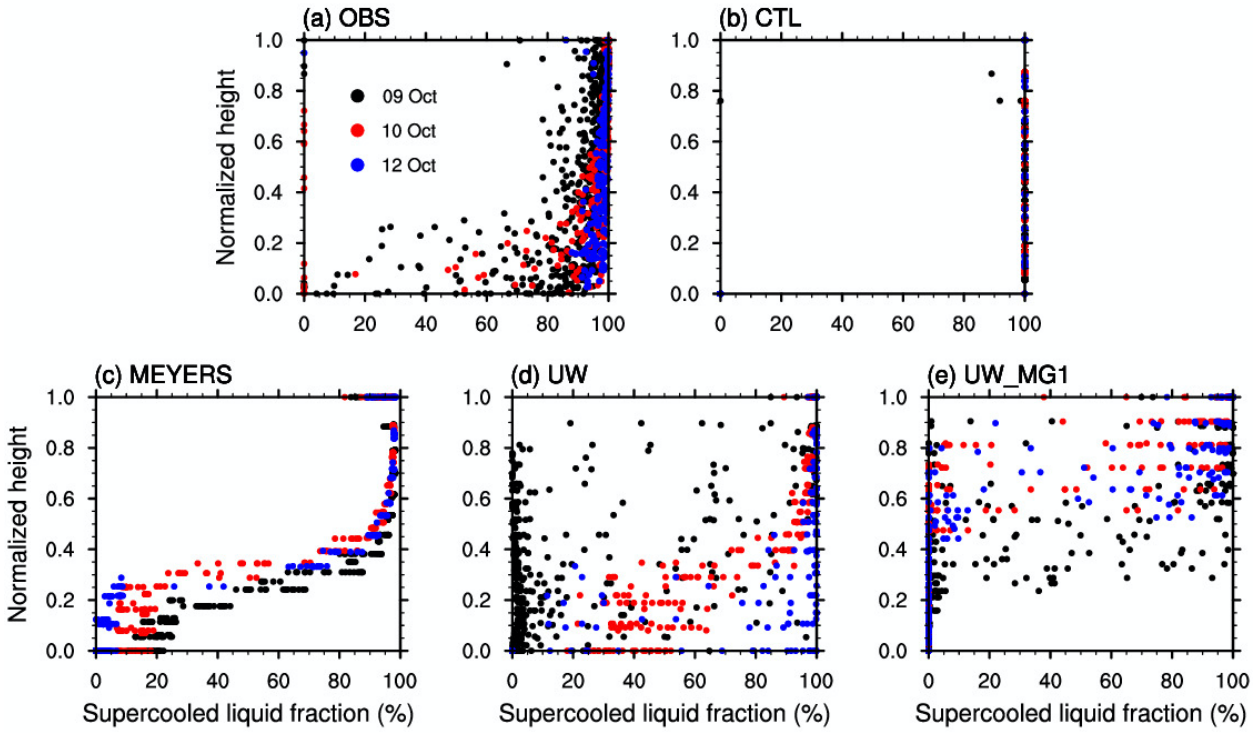

Figure 5. Distribution of supercooled liquid fraction as a function of normalized height in clouds. (a) The in-situ measurements obtained from the University of North Dakota Citation aircraft (McFarquhar et al., 2007) on 9 October (black dots), 10 October (red dots), and 12 October (blue dots) during the M-PACE field campaign. (b)-(e) Results of model simulations from CTL, MEYERS, UW, and UW_MG1, respectively. Model results are sampled on 9, 10, 12 October which correspond to the same time period as the measurements.

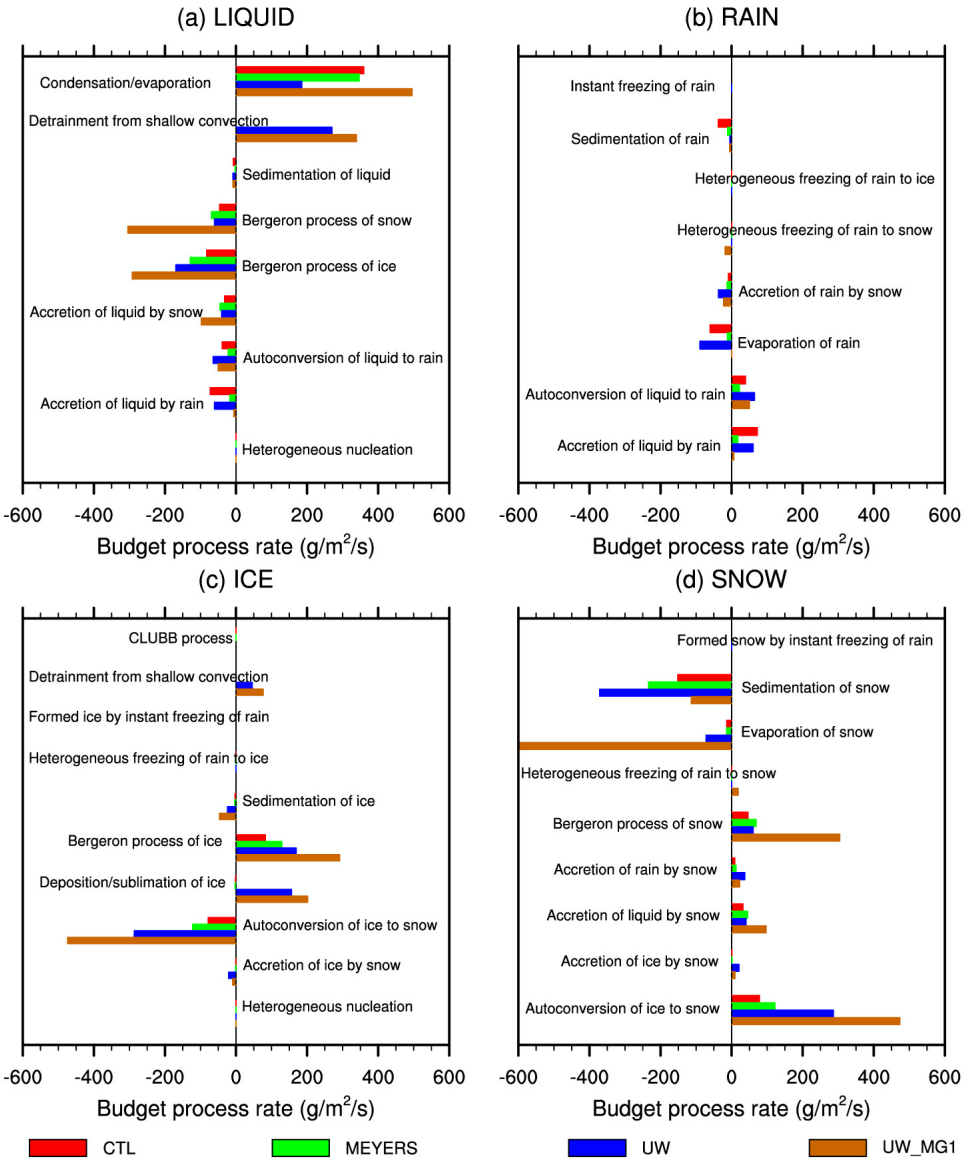

Figure 6. Budgets of vertically integrated cloud physical process tendencies of (a) cloud liquid, (b) rain, (c) cloud ice, and (d) snow hydrometeors from the short-term hindcast day-2 results of CTL (red bars) and three sensitivity experiments, which are MEYERS (green bars), UW (blue

67 bars), and UW_MG1 (brown bars). The vertically integrated process rates are averaged over 3-
68 day period between 9 and 11 October 2004 during the M-PACE field campaign.